Ferroelectricity of Sn-doped SrTiO$_3$ perovskites with tin at both *A* and *B* sites

Shoichiro Suzuki,[1,*] Atsushi Honda,[1] Naoki Iwaji,[1] Shin'ichi Higai,[1] Akira Ando,[1] Hiroshi Takagi,[1]
Hirofumi Kasatani,[2] and Kiyoshi Deguchi[2]

[1]*Murata Manufacturing Company, Limited, Nagaokakyo, Kyoto 617-8555, Japan*
[2]*Shizuoka Institute of Science and Technology, Fukuroi, Shizuoka 437-8555, Japan*

We successfully obtained Sn-doped SrTiO$_3$ (SSTO) perovskites, and clarified their ferroelectricity and structural properties by using first-principles theoretical calculations. The ferroelectricity of SSTO was confirmed by the appearance of a dielectric permittivity maximum and a clear hysteresis loop of the relationship between the external electric field and the electric flux density below 180 K. X-ray diffraction and Raman spectra revealed the structural phase transition of SSTO at approximately 200 K. We directly observed by spherical aberration corrected scanning transmission electron microscopy with energy-dispersive x-ray spectroscopy that Sn ions are doped into both Sr and Ti sites (Sn$_A$ and Sn$_B$), and that Sn$_A$ is located at an off-centered position. We also performed theoretical analyses of SSTO and related perovskites, and found that Sn$_A$ is preferentially located in an off-centered position and that Sn$_A$ and the O$_6$ octahedron, which includes Sn$_B$ in its center, oscillate along the antiphase direction in the soft mode. Thus, we propose that the ferroelectricity of SSTO originates from the antiphase off-centering, which induces ferroelectric nanoregions in paraelectric SrTiO$_3$.

PACS number(s): 77.84.Cg, 77.80.B−, 61.72.−y, 71.15.Mb

It is well known that ferroelectric perovskite oxides (ABO_3) are important materials for both basic materials science and the applied electronics industry. The substitution of Sn ions into the *A* sites of the perovskite lattice has recently been a subject of intensive research, because this is a promising approach for the fabrication of Pb-free ferroelectric materials.[1–4] However, the synthesis of ferroelectric ABO_3 substituted Sn ions for the *A* sites was found to be difficult in experimental studies.[5,6]

Recently, we succeeded in obtaining ferroelectric perovskites in which Sn ions were doped into the *A* sites. We fabricated Sn and Ca codoped ferroelectric BaTiO$_3$ (BTO), which exhibited a higher phase transition temperature than undoped BTO.[7,8] Further, we theoretically confirmed the efficiency of codoping by using first-principles calculations.[9] We showed that Ca doping results in a decrease of lattice size, which promotes Sn doping.

In this Rapid Communication, we choose paraelectric SrTiO$_3$ (STO) and doped Sn into it for the following reasons. First, the lattice size of STO is smaller than BTO. Moreover, STO exhibits quantum paraelectricity, which originates from quantum fluctuations.[10] Therefore, it is very sensitive to extrinsic conditions, such as ion substitution,[11–13] uniaxial stress,[14] and ^{18}O anion doping,[15] which all induce ferroelectricity. Here we explain the composition of Sn-doped STO (SSTO) perovskites. Then, we describe our experimental and theoretical examinations of their ferroelectricity and structural properties. In particular, we report atomic scale observations of SSTO obtained by using spherical aberration corrected scanning transmission electron microscopy (Cs-STEM) along with energy-dispersive x-ray spectrometry (EDS). We discuss the relation between the phonon properties and ferroelectricity of SSTO, and propose the origin of its ferroelectricity.

Calcined powder of SSTO was obtained by a solid state reaction, and the powder and an organic binder were mixed and pressed to the green body. Then, square SSTO ceramic plates, 2.0 × 2.0 × 0.5 mm^3 in size, were obtained by a conventional sintering process during which the partial pressure of oxygen gas was controlled.[7,8] We defined the composition of SSTO to be $(Sr_{1-a}Sn_a)(Ti_{1-b}Sn_b)O_3$, where *a* and *b* are the concentrations of Sn at Sr and Ti sites, respectively. The total concentration of Sn in SSTO is defined as $x = a + b$, and *x* was within the range of $0 − 0.1$ in the present study. The dependencies of the dielectric properties on temperature were investigated using an impedance analyzer (HP-4194A, Agilent). The existence of a ferroelectric phase was verified by analyzing the relationship between the external electric field and the electric polarization using a ferroelectric tester (Precision Premier II, Radiant Technologies). The pyroelectricity was measured with an electrometer (8252 digital electrometer, ADCMT). The x-ray diffraction (XRD) profiles (Huber 424 + 511.1: MXCH-18, Mac Science) and Raman spectra (NRS-3300, JASCO) were analyzed in order to clarify the existence of a structural phase transition with temperature. The atomic scale morphological observations were carried out at room temperature using Cs-STEM (JEM-ARM200F, JEOL), and the locations of Sn ions were determined with an EDS (JED-2300T, JEOL), which was attached to the Cs-STEM. The phonon frequencies and eigendisplacements of cubic STO, SnTiO$_3$, SrSnO$_3$, and SnSnO$_3$ were obtained by first-principles calculations using the Vienna *ab initio* simulation package (VASP) code[16] in order to discuss the relationship between the dielectric properties and structural phase stability.

The relationship between the real part of the dielectric permittivity (ε'), the frequency of the external electric field (f), and the temperature (T) is shown in Fig. 1 for SSTO with various concentrations (x) of Sn. A maximum of ε' was not observed over the entire range of temperature for the samples with $x = 0$. This is known as the quantum paraelectricity of STO. However, for $x > 0.02$, at a certain temperature T_m, there is a maximum $\varepsilon'(T_m)$ and T_m increases with increasing x. This is a similar result to our previous studies on Sn-doped BTO,[7,8] and we suggest that the ferroelectricity is due to the introduction of Sn ions into STO. In addition, the ε' at T_m
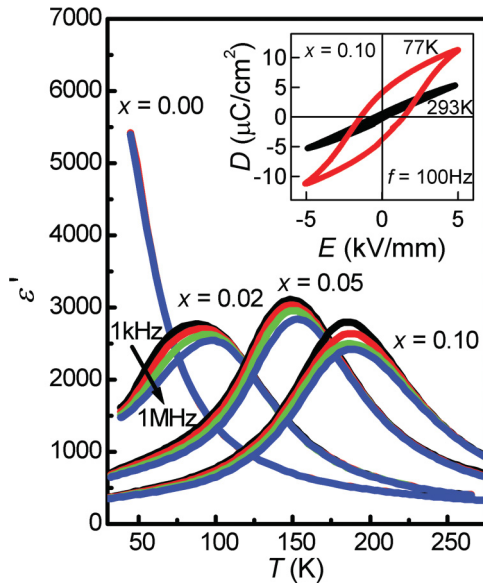
FIG. 1. (Color online) Dielectric and ferroelectric properties of SSTO with various concentrations (x) of Sn. The temperature dependencies of the real part of the dielectric permittivity were measured at 10^3–10^6 Hz. The inset shows the D-E relationship for 100 Hz at 77 and 293 K.

FIG. 2. (Color online) Structural transition of SSTO for $x = 0.10$. (a) The temperature dependence of the cubic lattice constant, which was calculated by using the (011), (002), and (112) reflections of XRD profiles. (b) Temperature evolution of the Raman spectra. Arrows show the vibrational modes that disappear above 200 K.

for $x = 0.02$ varies with frequency. This shows that STO is transferred to a relaxor state from a paraelectric state. However, the ε' at T_m for $x > 0.05$ is not varied with frequency. So we concluded that the ferroelectricity appears explicitly with increasing the amount of Sn ions in STO.

The relationship between the external electric field (E) and the electric flux density (D) of SSTO with $x = 0.1$ at $T = 77$ and 293 K, i.e., below and above T_m, respectively, are shown in the inset of Fig. 1. Using P and E, D is defined as $D = \varepsilon_0 E + P$, where ε_0 is the permittivity of the vacuum. Although paraelectricity was observed at $T = 293$ K and there is an almost linear relationship between E and D, a hysteresis loop appeared at $T = 77$ K, which indicates the ferroelectric nature of the SSTO. In addition, the dielectric permittivity of SSTO with $x = 0.1$ followed a classical Curie-Weiss law $\varepsilon' = C/(T - \theta)$, where C is a constant and θ is the Curie-Weiss temperature, which corresponds to the transition temperature between the ferroelectric and paraelectric states. We then found that θ was approximately 200 K for $x = 0.1$. Thus, it was confirmed that a ferroelectric state of STO can be obtained by introducing Sn ions into the lattice.

It is known that the ferroelectric to paraelectric transition occurs along with a structural phase transition in perovskite-type crystal structures. The dependence of the lattice constant on temperature for SSTO ($x = 0.1$) was examined using XRD and is shown in Fig. 2(a). It was found that SSTO has a cubic symmetry at $T = 273$ K. The lattice constants (a) at all other temperatures were also calculated assuming cubic symmetry, and an inflection point was found at $T = 200$ K after using a least squares method to fit a linear equation to the measured a values. The temperature dependence of the Raman spectra is shown in Fig. 2(b), and was used to verify the structural phase transition. Two vibrational modes were observed at 200 and 550 cm^{-1} for $T \leqslant 200$ K, and these both disappeared at
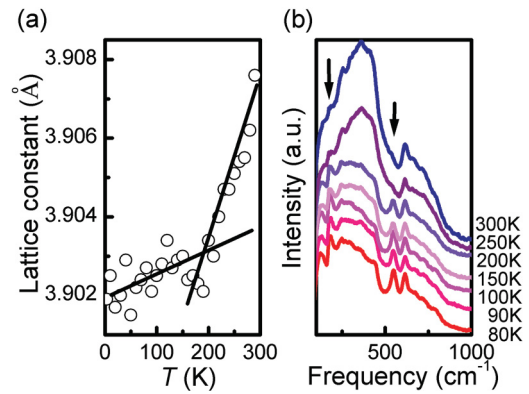
$T \geqslant 250$ K. Thus, by using two different experimental structure analyses, the structural phase transition of SSTO ($x = 0.1$) was confirmed to be around $T = 200$ K.

We also carried out direct observations of SSTO at an atomic scale by means of Cs-STEM combined with EDS, in order to distinguish the location of Sn ions. The $\langle 100 \rangle$ projection of a microstructural image of SSTO ($x = 0.1$) with a spatial resolution of 0.2 nm is shown in Fig. 3(a). The cations are distinguishable as bright spots, and the order of the Sr and Ti sites alternated. The inset of Fig. 3(a) shows the EDS intensities from the Sr L, Ti K, and Sn L edges, and they are shown in Fig. 3(b) as line profiles. The integration time of the x-ray scan for each element was 500 ms, and the increment of each scan step was 0.05 nm. It is found from Fig. 3(b) that Sn ions are located at both Sr and Ti sites. Furthermore, the Sn ions at Sr sites are located 0.05 nm from the site center, whereas Sn ions at Ti sites are located at the site center.

The contribution of Sn ions at Sr and Ti sites in STO, which we refer to as Sn$_A$ and Sn$_B$, respectively, to the dielectric properties and the structural stability is discussed by understanding the dynamical properties as represented by phonon modes. We performed first-principles calculations for STO, SnTiO$_3$, SrSnO$_3$, and SnSnO$_3$ with cubic Pm-$3m$ symmetry, and obtained phonon frequencies and eigendisplacements by calculating the force constants of atoms using density functional perturbation theory.[17] The optical modes at the Brillouin zone center with the lowest phonon frequencies, which govern the ferroelectricity of the perovskite crystal, are shown in Fig. 4(a). The vertical axis denotes the normalized eigendisplacements of each atom, and the corresponding phonon frequencies are also shown in Fig. 4(a). Imaginary phonon frequencies, which relate to the structural instability of the uniaxial deformations of the cubic lattice, were found in STO, SnTiO$_3$, and SnSnO$_3$. Then it is shown that they intrinsically have a ferroelectric nature and off-centered characteristics of Sn$_A$ or Sn$_B$. The eigendisplacement of the ABO_3 perovskite at the Brillouin zone center is represented by a combination of three standard vibrational modes, as represented schematically in Fig. 4(b). The first is the Slater mode,[18] which has an antiphase vibration of B and O$_6$ octahedral cages. The second is the Last mode,[19]
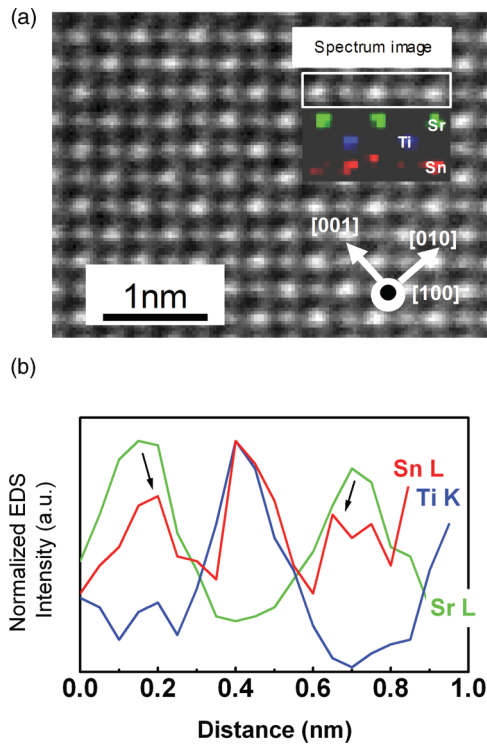
FIG. 3. (Color online) Cs-STEM and EDS analysis of SSTO for $x = 0.10$. (a) The Cs-STEM image of the SSTO grain that was recorded along the crystallographic $\langle 100 \rangle$ direction. The inset shows the distribution of the Sr (green), Ti (blue), and Sn (red) atoms, which were determined by EDS analysis. (b) Line profile of EDS intensity for the Sr L, Ti K, and Sn L edges as a function of scanning distance.

FIG. 4. (Color online) (a) Theoretically calculated eigendisplacement of phonons at the Brillouin zone center, for the lowest frequencies of the optical modes. The corresponding phonon frequencies are shown at the bottom. (b) Schematic representation of three standard vibrational modes at the Brillouin zone center, which were drawn using the VESTA visualization software (Ref. 23).

which corresponds to an antiphase vibration of A and BO_6 octahedra. The third corresponds to the uniaxial deformation of the O_6 octahedral cage, and is referred to as the Axe mode.[20] The eigendisplacement of STO shows the antiphase vibration of B and O atoms, whereas the displacement of A is smaller. This displacement is predominantly due to the Slater mode, and this theoretical result corresponds to experimental results.[21] In the case of SnTiO$_3$, the antiphase displacement of both A and B against O was clearer than in STO, as shown in Fig. 4(a). We also found that the concentration of the Last mode increased by substituting Sn ions for Sr sites in STO,[22] and that the off-centering of Sn$_A$ is observable when the vibrations corresponding to the Last mode are frozen by reducing the temperature. In contrast, it is found that there was little contribution of the Slater mode to the eigendisplacement of SrSnO$_3$ and SnSnO$_3$, whereas the magnitude of the Last mode was considerable. Furthermore, there is a significant contribution from the Axe mode, and larger differences between the eigendisplacements of O_x ($=O_y$) and O_z were exhibited compared to those found in STO and SnTiO$_3$. The off-centering of the A site ions is not observed in SrSnO$_3$ but in SnSnO$_3$, because only the latter has an imaginary frequency associated with its eigendisplacement. We then conclude from the theoretical results that only the coexistence of Sn$_A$ and Sn$_B$ in STO results in the off-centering of A site ions while B site ions remain at the site centers. Thus, the location of Sn ions in STO and the off-centering of A site ions, which were observed by Cs-STEM analysis (Fig. 3), were verified theoretically.

Here, we discuss how Sn$_A$ affects the ferroelectricity and phase transition of STO. First, we have shown that Sn$_A$ is located at an off-centered position by using the Cs-STEM analysis (Fig. 3). The off-centering introduces a local dipolar distortion around the Sn$_A$ ions. The local dipolar distortion induces another dipolar distortion in the adjoining unit cells of the nonpoled, host STO lattice. Because STO is sensitive to extrinsic distortion, STO prefers the antiphase distortion between the Ti and O_6 octahedral cage, which results in a loss of the centrosymmetry of the cubic structure. This was demonstrated by our theoretical calculations of the eigendisplacement of phonons at the zone center for STO (Fig. 4). These dipolar distortions certainly lead to the formation of polar nanoregions with invertible spontaneous polarization of P_s around Sn$_A$.[24]

However, P_s of SSTO was not observed at room temperature where there is a linear relationship between E and D (Fig. 1). Assuming that P_s was too small to be detected by the D-E hysteresis, a pyroelectric analysis, which is more sensitive, was employed to detect P_s (Fig. 5). It was then found that an invertible P_s appears below room temperature and increases with decreasing temperature. The existence of P_s is evidence of the formation of polar nanoregions, which originate from the off-centered Sn$_A$ in the nonpolar STO lattice.

This also indicates that polar nanoregions grow with decreasing temperature as P_s increases. The decreasing temperature inevitably gives rise to the distortion of the STO lattice,
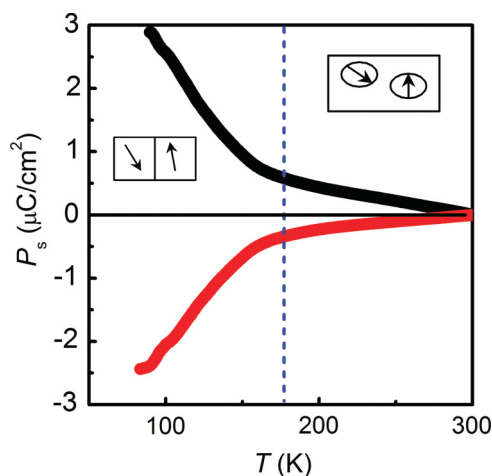
FIG. 5. (Color online) The invertible spontaneous polarization P_s as a function of temperature analyzed by the pyroelectric measurement. The dashed line shows the inflection temperature of P_s around 180 K. The insets are schematic images of dipoles below and above the inflection temperature, which is consistent with T_m and the structural phase transition temperature.

and thus it strengthens the dipolar distortions around Sn_A and leads to extended polar regions. These polar regions percolate through the entire STO lattice at lower temperatures, e.g., below 180 K, and then STO finally undergoes a cooperative ferroelectric phase transition.

Our discussion is consistent with the structural phase transition of SSTO shown in Fig. 2 and the rapid increase of P_s at $\leqslant$ 180 K shown in Fig. 5. Thus, we conclude that off-centered

Sn_A induces ferroelectric polar regions in paraelectric STO, and the growth of these regions results in the structural phase transition and the appearance of ferroelectricity. Our conclusion is consistent with the physical picture of relaxor ferroelectrics reported by Samara.[25]

In summary, we have shown that SSTO perovskites were successfully compounded, and their ferroelectricity and structural properties were clearly determined through experiments and theoretical calculations. We confirmed the ferroelectricity of SSTO by the appearance of a dielectric permittivity maximum and a clear D-E hysteresis loop below 180 K. A structural phase transition around 200 K was revealed by XRD and Raman spectra. By using Cs-STEM and EDS, it was shown that Sn ions are doped into both Sr and Ti sites, and that Sn_A is located at an off-centered position. We also examined theoretically the structural properties of SSTO and related perovskites, and found that Sn_A is preferentially located in an off-centered position and that Sn_A and the O_6 octahedron, which includes Sn_B in its center, oscillate along the antiphase direction in the soft mode. Accordingly, we proposed that the ferroelectricity of SSTO has its origin in the antiphase off-centering. That is, the antiphase off-centering induces ferroelectric polar regions in paraelectric STO, whose growth results in the structural transition and ferroelectricity. Such a unique origin of ferroelectricity opens up possibilities for high polarization materials design.

*shoichiro_suzuki@murata.co.jp

[1] Y. Uratani, T. Shishidou, and T. Oguchi, Jpn. J. Appl. Phys. **47**, 7735 (2008).

[2] J. W. Bennett, I. Grinberg, P. K. Davies, and A. M. Rappe, Phys. Rev. B **83**, 144112 (2011).

[3] R. Armiento, B. Kozinsky, M. Fornari, and G. Ceder, Phys. Rev. B **84**, 014103 (2011).

[4] W. D. Parker, J. M. Rondinelli, and S. M. Nakhmanson, Phys. Rev. B **84**, 245126 (2011).

[5] S. Matar, I. Baraille, and M. Subramanian, Chem. Phys. **355**, 43 (2009).

[6] T. Fix, S. L. Sahona, V. Garcia, J. L. MacManus-Discoll, and M. G. Blamire, Cryst. Growth Des. **11**, 1422 (2011).

[7] S. Suzuki, T. Takeda, A. Ando, and H. Takagi, Appl. Phys. Lett. **96**, 132903 (2010).

[8] S. Suzuki, T. Takeda, A. Ando, T. Oyama, N. Wada, H. Niimi, and H. Takagi, Jpn. J. Appl. Phys. **49**, 09MC04 (2010).

[9] S. Suzuki, A. Honda, S. Higai, A. Ando, N. Wada, and H. Takagi, Jpn. J. Appl. Phys. **50**, 09NC11 (2011).

[10] K. A. Müller and H. Burkard, Phys. Rev. B **19**, 3593 (1979).

[11] J. G. Bednorz and K. A. Müller, Phys. Rev. Lett. **52**, 2289 (1984).

[12] V. V. Lemanov, E. P. Smirnova, P. P. Syrnikov, and E. A. Tarakanov, Phys. Rev. B **54**, 3151 (1996).

[13] V. V. Lemanov, E. P. Smirnova, and E. A. Tarakanov, Phys. Solid State **39**, 628 (1997).

[14] H. Uwe and T. Sakudo, Phys. Rev. B **13**, 271 (1976).

[15] M. Itoh, R. Wang, Y. Inaguma, T. Yamaguchi, Y. J. Shan, and T. Nakamura, Phys. Rev. Lett. **82**, 3540 (1999).

[16] G. Kresse and J. Furthmuller, Phys. Rev. B **54**, 11169 (1996).

[17] X. Gonze and C. Lee, Phys. Rev. B **55**, 10355 (1997).

[18] J. C. Slater, Phys. Rev. **78**, 748 (1950)

[19] J. T. Last, Phys. Rev. **105**, 1740 (1957).

[20] J. D. Axe, Phys. Rev. **157**, 429 (1967).

[21] J. Harada, J. D. Axe, and G. Shirane, Acta Crystallogr. A **26**, 608 (1970).

[22] J. Hlinka, J. Petzelt, S. Kamba, D. Noujni and T. Ostapchuk, Phase Transitions **79**, 41 (2006).

[23] K. Momma and F. Izumi, J. Appl. Crystallogr. **44**, 1272 (2011).

[24] G. Burns and F. H. Dacol, Phys. Rev. B **28**, 2527 (1983).

[25] G. Samara, J. Phys.: Condens. Matter **15**, R367 (2003).